Modelling of Residual Stresses and Distortions of the Wall on a Substrate Built by Wire-Arc Surfacing

Dmitriy S. Dudin[*]
Ilya E. Keller[†]
Institute of Continuous Media Mechanics of UB RAS
Perm National Research Polytechnic University
Perm, Russian Federation
Gleb L. Permyakov[‡]
Dmitriy N. Trushnikov[§]
Perm National Research Polytechnic University
Perm, Russian Federation

Abstract. To study the arising of technological distortions and residual stresses in structures created by wire-arc surfacing, it is proposed to consider a wall consisting of ten layers deposited on a substrate. A wall is deposited with and without layer-by-layer forging on a fixed steel plate with AISI 308 LSi austenitic stainless steel wire and the deflection of a released wall on the substrate is measured. As for numerical modelling, the process was presented as successively solved problems: a) thermal — surfacing of ten layers of material, b) elastic-plastic — formation of eigenstrains and residual stresses due to cooling of the created structure with nonuniformly distributed temperature, c) thermo-elastic-plastic — forging of the workpiece with a pneumatic tool at elevated temperature (this stage may be excluded) and d) elastic-plastic — the structure distortion and changes in the field of residual stresses when the structure is released. Problems (a), (b), (d) were solved in the COMSOL Multiphysics software package, (c) — in LS-DYNA. It is established that tensile residual stresses are formed in the deposited wall near its upper face, and the forging of this face is accompanied by a decrease in longitudinal strains, distortion of the released specimen and inhomogeneity of the distribution of residual stresses by the wall height. The calculated deflection values correspond to our experimental data and the results of Cranfield University for the IN718 austenitic alloy. A rod-beam model of the built-up multilayer wall was developed, the results of the application of which correspond to numerical calculations.

Keywords: wire-arc surfacing, layer-by-layer forging, residual stresses, distortions, experiment, mathematical model.

Citation: D.S. Dudin, I.E. Keller, G.L. Permyakov, D.N. Trushnikov, Modelling of Residual Stresses and Distortions of the Wall on a Substrate Built by Wire-Arc Surfacing, J. Sib. Fed. Univ. Math. Phys., 2024, 17(1), 75–90. EDN: VUNMCP.

Introduction

Wire-arc additive manufacturing creates lightweight, rigid and durable metal structures of irregular shapes with significant material savings. It appears that the first direct predecessor of

[*]dmitryovj@yandex.ru   https://orcid.org/0000-0002-1911-8899
[†]kie@icmm.ru   https://orcid.org/0000-0001-9914-8870
[‡]gleb.permyakov@yandex.ru   https://orcid.org/0000-0001-8158-3460
[§]trdimitr@yandex.ru   https://orcid.org/0000-0001-7105-7934

this method was the electric casting of metals for the restoration of machine parts developed in 1888 by N. G. Slavyanov, assistant mining chief of the Perm Cannon Plants, who was awarded a medal at the World Electrotechnical Exhibition in Chicago in 1893 (the exhibit included a hexagonal "glass" deposited from bell bronze, tombac, nickel, steel, cast iron, copper, nickel silver and bronze layers, kept in the memorial house-museum of N. G. Slavyanov in Perm; another glass made for the IV Electrical Exhibition in St. Petersburg in 1892, kept in the Historical and Technical Museum of Peter the Great St. Petersburg Polytechnic University). Modern wire-arc additive manufacturing methods based on efficient technologies (plasma, plasma-arc with consumable electrodes and cold metal transfer) with layer-by-layer point pressure or thermomechanical treatment have been developed in the last ten years by such scientific organisations as Cranfield University, the University of Manchester and the University of Queensland [1, 2], the Indian Institute of Technology Bombay [3], the Beijing Institute of Technology, Perm National Research Polytechnic University [4, 5], Bryansk State Technical University [6] and Tomsk Polytechnic University. Additive manufacturing technologies with layer-by-layer treatment using a pneumatic impact tool or roller run-in can create a correct microstructure and related material strength and plasticity, as well as minimise the nonuniform distribution of residual stresses and strains of the erected structure.

This article is aimed at understanding the regularities of formation of the stress-strain state of a structure built up by wire-arc surfacing with and without layer-by-layer forging. As a reference specimen, the authors [7] proposed to consider a structure of certain dimensions consisting of a wall of 10 layers deposited on a substrate (a steel plate fixed on a rigid horizontal surface). They studied the deflection and wall height distribution of the main components of residual stresses of a released structure for aluminum, titanium, nickel alloys and mild steel deposited on a substrate, with and without layer-by-layer roller running-in. It has been found that layer-by-layer point pressure treatment can reduce structural distortions several times; at the same time, the change in residual stress distribution turns out to be quite intricate. In the present work, 10 layers of austenitic stainless steel (AISI 308 LSi) with and without layer-by-layer forging by a pneumatic tool were deposited on a "standard" substrate, and the deflection of the substrate was measured after it was released from fastening. The same problem was studied numerically. The calculation results were compared with the experimental ones obtained by us and the authors [7] for the IN718 nickel-based austenitic alloy. The verified numerical model made it possible to understand the mechanism of evolution of structural strains and residual stresses during wall surfacing on the substrate and the role of layer-by-layer forging in this evolution, depending on the process parameters. To study the evolution of strains related to the reference built-up specimen in terms of the mechanics of the growing body, a simplified scheme of the specimen as rods/beams package was considered and relations were derived to assess the bending and distribution of residual stresses over the package thickness. When applied to the reference specimen, these relations assess the acceptability of an unrelated (or the expediency of considering a related) formulation of the thermo-elasto-plasticity problem for numerical modelling of the hybrid additive manufacturing process.

1.   Experimental part

The wall consisting of ten material layers was deposited on the substrate (a rectangular plate $180 \times 50 \times 5$ mm made of 12Chr18Ni10Ti steel) fastened in the horizontal table of the automatic hybrid additive manufacturing installation at eight points. The AISI 308 LSi wire of 1.2 mm in

diameter and the cold metal transfer technology with layer surfacing along the zigzag trajectory of $\pm 45°$ were used. The surfacing speed 8.3 mm/s of the layer of 150 mm in length and the pause 150 s between the surfacing passes were set. The wall with layer-by-layer forging in one pass was welded onto the second plate in the same way. The forging was carried out using the SA7401H AIRPRO pneumatic hammer mounted on the installation column and equipped with a head and a spherical tip of 15 mm in radius. The standard working pressure of 0.6 MPa, the pressure of the head pressure of 0.2 MPa and the feed rate of 3.3 mm/s were used, thereby ensuring the uniformity of the workpiece processing.

Photo of a specimen is shown in Fig. 1. The average height and cross-section width of the wall deposited without forging were 19.0×8.5 mm, deposited with layer-by-layer forging — 16.1×9.7 mm. The deflection of the structure released from fastening was 1.95 mm without
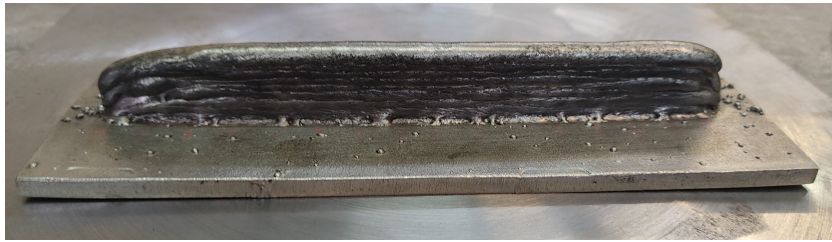

Fig. 1. Deflection of the substrate with a deposited edge without layer-by-layer forging

layer-by-layer forging and 1.58 mm with it. The deflection of the substrate pressed by the clamp in the specimen centre was measured using a marking gauge at its two extreme points along the surfacing line, as in [7]. It is appropriate to refer here to these works [7] related to the IN718 austenitic inconel alloy. The deflection of the released structure was 3.61 mm without layer-by-layer roll-in and 0.99 mm with it. There were some differences in the experiment organisation, such as: the substrate was made of the same material (inconel IN718) and had dimensions of $200 \times 64 \times 6$ mm, 9 layers were deposited without layer-by-layer roll-in and 11 ones with it, and the corresponding height h and width b of the wall section were 22.6×6.9 mm and 20.9×8.0 mm. The given transverse dimensions allow us to compare the intensity of pressure treatment: 14.1% of linear strain $\epsilon = (b_p - b)/b$ (the index "p" corresponds to layer-by-layer pressure treatment) for AISI 308 LSi and 16.0% for IN718. The curvature of the substrate $\kappa \approx 8D/L^2$, where L is its length and D is the deflection gives values of 0.48 for AISI 308 LSi and 0.72 for IN718. These values allow us to conclude that the roller run-in in [7] provided a slightly higher intensity of pressure treatment than the forging in our experiment.

2. Elastic beam-rod model of distortions and residual stresses in the built-up specimen

To evaluate the deflection of the built-up linear segment, an elastic beam-rod model was developed, within which the equilibrium problems of n deposited layers and the substrate a) as rods and b) as beams are solved one by one. It is assumed that after surfacing the next layer, the temperature profile shifts towards the free boundary by the amount of the layer thickness h. The temperature profile is described by a series T_i, $i = 1, \ldots, n + 1$, the values of which are attributed to the layers. Further, the indices mean: i is the number in the temperature series, starting from the top layer $i = 1$ to the substrate $i = n + 1$, k is the layer number, starting

from the substrate $k = 0$ to the top layer $k = n$. At the first stage, the layers are taken by rods. Let us call $\epsilon_i^t = \alpha(T_i - T_{amb})$, $i = 1, \ldots, n+1$ as temperature strains of the rod with length l, where T_{amb} — ambient medium temperature, then the strain of the rod package consisting of the substrate and the n deposited layers are equal to

$$\epsilon_n = \frac{F/f\epsilon_{n+1}^t + \sum\limits_{j=1}^{n} \epsilon_j^t + \sum\limits_{j=1}^{n} \epsilon_j^h + n\epsilon^p}{n + F/f}, \quad n \geqslant 1, \tag{1}$$

$$\epsilon_0^h = 0, \quad \epsilon_1^h = \epsilon_2^t, \quad \epsilon_n^h = \frac{F/f\epsilon_{n+1}^t + \sum\limits_{j=2}^{n} \epsilon_j^t + \sum\limits_{j=1}^{n-1} \epsilon_j^h + (n-1)\epsilon^p}{n - 1 + F/f}, \quad n \geqslant 2, \tag{2}$$

where F and f are the cross-sectional areas of the substrate and the layer, ϵ_k^h, $k = 0, \ldots, n$ are the strains of the rods in the package consisting of the substrate and the $n - 1$ layers, induced by temperatures T_i, $i = 2, \ldots, n+1$.

The strain ϵ_n can also be obtained as a result of solving the equilibrium problem of the elastic rod package with eigenstrains

$$\epsilon_{0,n}^{eig} = \epsilon_{n+1}^t, \quad \epsilon_{k,n}^{eig} = \epsilon_k^h + \epsilon_{n-k+1}^t + \epsilon^p, \quad k = 1, \ldots, n, \tag{3}$$

where $\epsilon_{0,n}^{eig}$ and $\epsilon_{k,n}^{eig}$ is eigenstrains in the substrate and in the k-th layer after surfacing the n layers. Plastic strains of layer-by-layer pressure treatment should be added to the eigenstrains (3).

Expressions (1),(2) were obtained by sequentially solving two problems (Fig. 2) for each value $n \geqslant 1$:

1. Calculation of strains ϵ_n^h from the system of equations $\sum\limits_{k=0}^{n-1} P_{k,n}^h = 0$, where $P_{0,n}^h = EF(\epsilon_n^h - \epsilon_{n+1}^t)$, $P_{k,n}^h = Ef(\epsilon_n^h - (\epsilon_k^h + \epsilon_{n-k+1}^t + \epsilon^p))$, $k = 1, \ldots, n-1$.

2. Attaching another layer with temperature T_1 and the length $l(1 + \epsilon_n^h)$ to the package and cooling them to the temperature T_{amb}. The strain of the package ϵ_n are determined from the system of equations $\sum\limits_{k=0}^{n} P_{k,n} = 0$, where $P_{0,n} = EF(\epsilon_n - \epsilon_{n+1}^t)$, $P_{k,n} = Ef(\epsilon_n - (\epsilon_k^h + \epsilon_{n-k+1}^t + \epsilon^p))$, $k = 1, \ldots, n$.
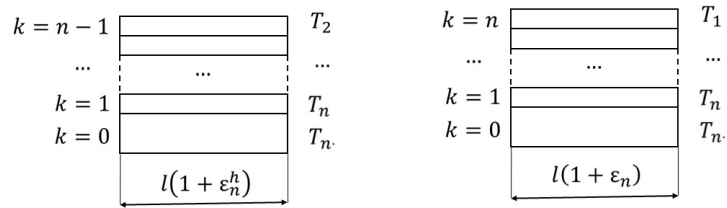

Fig. 2. Schemes of the first and second problems for a package of rods

At $n = 1$ at the first stage we find $\epsilon_1^h = \epsilon_2^t$ from the equations $P_{0,1}^h = EF(\epsilon_1^h - \epsilon_2^t)$, $P_{0,1}^h = 0$, at the second one we find ϵ_1 from the equations $P_{0,1}^h = EF(\epsilon_1 - \epsilon_2^t)$, $P_{1,1} = Ef(\epsilon_1 - (\epsilon_1^h + \epsilon_1^t + \epsilon^p))$, $P_{0,1} + P_{1,1} = 0$. The problems for the next n are solved taking into account the results of solving the previous ones, from which the values ϵ_k^h, $k = 1, \ldots, n-1$ are determined.

The forces in the rods are determined using the expressions

$$P_{0,n} = E\frac{\sum\limits_{j=1}^{n} \epsilon_{j,n}^{eig} - n\epsilon_{0,n}^{eig}}{n/F + 1/f}, \quad P_{1,1} = E\frac{\epsilon_{0,1}^{eig} - \epsilon_{1,1}^{eig}}{1/F + 1/f}, \tag{4}$$

$$P_{k,n} = E \frac{\epsilon_{0,n}^{eig} - \epsilon_{k,n}^{eig} + f/F \left(\sum\limits_{j=1}^{n} \epsilon_{j,n}^{eig} - n\epsilon_{k,n}^{eig} \right)}{n/F + 1/f}, \tag{5}$$

following from the solution of the system $P_{0,n} = EF(\epsilon_n - \epsilon_{0,n}^{eig})$, $P_{1,n} = Ef(\epsilon_n - \epsilon_{1,n}^{eig})$, ..., $P_{k,n} =$
$= Ef(\epsilon_n - \epsilon_{k,n}^{eig})$, $k = 0, \ldots, n$, $\sum\limits_{j=0}^{n} P_{j,n} = 0$.

In a particular case, after cooling of the wall which instantly appeared with an inhomogeneous temperature profile in height, the expressions (1), (2) with $\epsilon_{k,n}^{h} = 0$, $k = 0, \ldots, n$, $\epsilon^p = 0$ take the view

$$\epsilon_n = \frac{F/f\epsilon_{n+1}^t + \sum\limits_{j=1}^{n} \epsilon_j^t}{n + F/f}, \quad n \geqslant 1, \quad \epsilon_{k,n}^{eig} = \epsilon_{n-k+1}^t, \quad 0 = 1, \ldots, n. \tag{6}$$

This case underestimates the heterogeneity of eigenstrains associated with the build-up incrementality, and will not be considered further.

According to the known longitudinal forces P_n^k, $k = 0, \ldots, n$ the deflection values of the specimen are determined, which is assumed by the Bernoulli–Euler beam (Fig. 3). The expression for the deflection amount w_n of the substrate with the n layers as a beam is as follows

$$w_n = \frac{l(L - l/2)}{8EJ_n} M_n, \tag{7}$$

$$J_n = \frac{b(nh)^3}{12} + bnh \left(\frac{H + nh}{2} - z_n \right)^2 + \frac{BH^3}{12} + BHz_n^2, \quad z_n = \frac{bnh(H + nh)}{2(BH + bnh)}, \tag{8}$$

$$M_n = \left(2P_{0,n}z_n - h \sum\limits_{j=1}^{n} (2k - 1)P_{j,n} - (H - 2z_n) \sum\limits_{j=1}^{n} (2k - 1)P_{j,n} \right) \tag{9}$$

where M_n and J_n are the bending moment and the moment of inertia of the cross section, z_n is the distance from the center of mass of the substrate to the center of mass of n deposited layers.
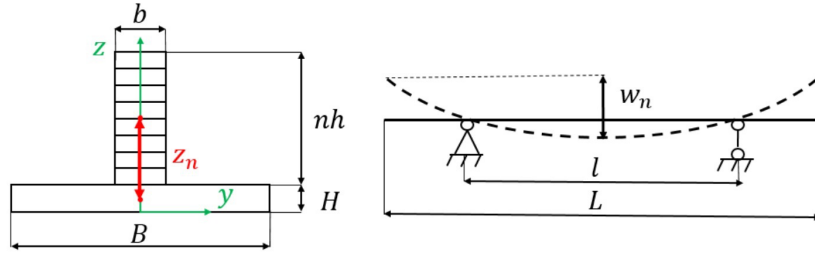

Fig. 3. Schemes of the problem of bending the wall being built up as a package of beams

For a more correct assessment of the distortion of the sample and residual stresses in it, it is necessary to take into account inelastic deformations, inhomogeneity of the distribution along the length of the stress-strain state of the segment and other subtle issues [8].

3.   Modelling the surfacing of the wall on a substrate

The following scheme was implemented to model the evolution of the temperature field distribution during the layer-by-layer surfacing of the wall on the substrate. As the next layer is
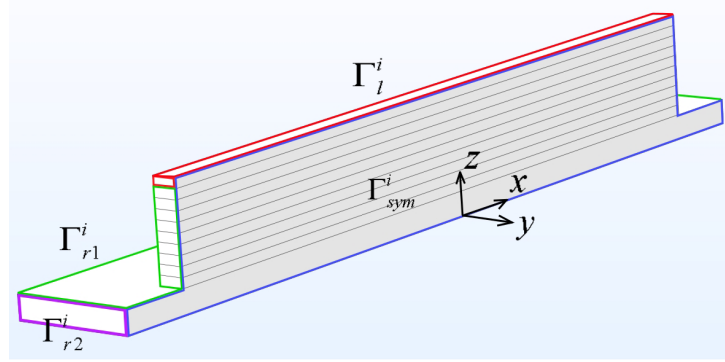
Fig. 4. Geometric model of the wall

surfaced, the volumes of the geometric model of the wall (Fig. 4) are gradually activated. To do so, the thermal conductivity coefficient of the wall material, which is identically equal to zero at the beginning of the process, takes a non-zero temperature-dependent value for the volumes through which the heat source has passed or in which it has been located. The heat source is localized in the volume of a rectangular parallelepiped $10 \times 10 \times 2$ mm along with $x \times y \times z$ coordinates moving at a speed of $v_x = 8.3$ mm/s along the deposited layer. The boundary between the positive and zero coefficients of thermal conductivity is smoothed using the error function

$$\lambda_l(x,t) = \frac{\lambda}{2} \left(1 - \mathrm{erf} \left(\frac{x - \mu_x(t)}{\sqrt{2\sigma_x^2}} \right) \right), \quad \boldsymbol{x} \in \Omega_l^i, \quad \mu_x(t) = \mu_x^0 + v_x t, \tag{10}$$

where $\boldsymbol{x}$ — radius-vector of a material point, Ω_l^i is the volume corresponding to the i-th deposited layer (l from "the layer"), to ensure the stability of the advancing temperature front. In the volume of the heat source in the i-th heated layer, its specific power is given by the expression

$$q_i = q_{zi}(z)q_x(x,t)q_T(T), \quad \boldsymbol{x} \in \{\Omega_l \cap x \geqslant -(l + l_{spot})/2 + v_x t\}, \tag{11}$$

$$q_{zi} = \frac{Q_{max} - Q_{min}}{z_i^{max} - z_i^{min}} z + \frac{Q_{min}z_i^{max} - Q_{max}z_i^{min}}{z_i^{max} - z_i^{min}}, \tag{12}$$

$$q_x(x,t) = \frac{1}{2} \left(1 - \mathrm{erf} \left(\frac{x - \mu_x(t)}{\sqrt{2\sigma_x^2}} \right) \right), \tag{13}$$

$$q_T(T) = \frac{1}{2} \left(1 - \mathrm{erf} \left(\frac{T - \mu_T}{\sqrt{2\sigma_T^2}} \right) \right), \tag{14}$$

where the function q_{zi} is responsible for the uniformity of heating of the i-th layer in height, T is the absolute temperature, q_T regulates the bath temperature, the maximum value of which is equal to the liquidus temperature $T_{liq} = 1788$ K, q_x is responsible for the uniformity of heating and the movement of the source area along the direction of surfacing, z_i^{min}, z_i^{max} are the minimum and maximum values of the z-coordinate of the i-th surfaced layer, $l = 150$ mm is the layer length, $l_{spot} = 10$ mm is the source spot length. The parameters of the regulatory functions in equations (10)–(14) were selected manually from the stability of the thermal front and the maximum permissible temperature value and are given in Tab. 1. Therefore, the problem

Table 1. Parameters of the regulatory functions

Notation	Unit	Value
σ_x	mm	0.8
μ_x^0	mm	−72.8
Q_{min}	W/m^3	240
Q_{max}	W/m^3	300
μ_T	K	1688
σ_T	K	313

of layer surfacing is reduced to that of layer heating by a moving source with a corresponding change over time in the profile of the thermal conductivity coefficient along the layer.

The thermal conductivity problem was numerically implemented in the COMSOL Multiphysics package using an implicit integration scheme with a time step of 0.01 s. The computational domain was divided by a uniform mesh of hexagonal quadratic finite elements. As a result of the study of the precision of calculation results based on the finite elements, the maximum size of the finite element side for the substrate is 1.7 mm, for the layers — 1 mm. The physical constants of AISI 308 LSi steel were taken for the wall material, those of carbon steel — for the substrate plate. For brevity, the equations were written using the same designations of mass density ρ, the thermal conductivity coefficient λ and the specific heat capacity c_p for both materials, but bearing in mind their difference in the areas of the computational domain. Ten layers of $150 \times 10 \times 2$ mm each were deposited on the substrate of $180 \times 50 \times 5$ mm. The temperature field resulting from the surfacing of the i-th layer was found when solving the non-stationary problem of thermal conductivity

$$\rho c_p \frac{\partial T}{\partial t} = \boldsymbol{\nabla} \cdot (\lambda_l \boldsymbol{\nabla} T) + q_i, \quad \boldsymbol{x} \in \Omega_l^i, \tag{15}$$

$$\rho c_p \frac{\partial T}{\partial t} = \boldsymbol{\nabla} \cdot (\lambda \boldsymbol{\nabla} T), \quad \boldsymbol{x} \in \Omega_r^i, \tag{16}$$

where ∇ is the Hamilton operator, q_i is the specific power of the heat source in the i-th deposited layer given by (10)–(14), Ω_r^i is the volume corresponding to the remaining material during heating of the i-th layer (r from "the rest"), with boundary and initial conditions

$$-\lambda_l \boldsymbol{n} \cdot \boldsymbol{\nabla} T = \epsilon_T \sigma_{SB}(T^4 - T_0^4) + k(T - T_0), \quad \boldsymbol{x} \in \Gamma_l^i, \tag{17}$$

$$-\lambda \boldsymbol{n} \cdot \boldsymbol{\nabla} T = \epsilon_T \sigma_{SB}(T^4 - T_0^4) + k(T - T_0), \quad \boldsymbol{x} \in \Gamma_{r1}^i, \tag{18}$$

$$\lambda_l \boldsymbol{n} \cdot \boldsymbol{\nabla} T = 0, \quad \boldsymbol{x} \in \Gamma_{r2}^i \cup \Gamma_{sym}^i, \tag{19}$$

$$T(t = 0) \equiv T_{rel}^i, \quad \boldsymbol{x} \in \Omega_i, \tag{20}$$

where $\boldsymbol{n}$ is the unit vector of the external normal to the boundary, Γ_l^i is the surface of the i-th heated layer, Γ_r^i is the surface corresponding to the remaining material during heating of the i-th layer, $\Omega^i = \Omega_l^i \cup \Omega_r^i$, T_{rel}^i — homogeneous temperature distribution after $(i-1)$-th layer deposition and relaxation. Boundary conditions (17), (18) are the conditions of radiation and convective heat exchange with the environment, (19) is the thermal insulation condition for Γ_{r2}^i and the symmetry condition for Γ_{sym}^i. At the boundary of the volumes Ω_l^i and Ω_r^i, the condition of continuity in temperature is provided. The remaining designations in (15)–(20) and the values of the corresponding physical constants are given in Tab. 2.

Table 2. Constants of the thermal conductivity model

Constant	Designation	Dimension	Value
Liquidus temperature of AISI 308 LSi	T_{liq}	K	1788
Ambient temperature	T_0	K	293
Specific heat capacity of AISI 308 LSi	c_p	J/kg/K	710
Specific heat capacity of the plate steel	c_p	J/kg/K	500
Mass density of AISI 308 LSi	ρ	kg/m^3	7680
Mass density of plate steel	ρ	kg/m^3	7800
Thermal conductivity coefficient of AISI 308 LSi	λ	W/m/K	26
Thermal conductivity coefficient of plate steel	λ	W/m/K	42
Coefficient of thermal radiation	ϵ_T	kg/m^3	0.8
Heat transfer coefficient	k	W/m^2/K^2	15
Stefan – Boltzmann constant	σ_{SB}	W/m^2/K^2	$5.67 \cdot 10^{-8}$

After surfacing the next layer, a non-stationary thermal conductivity problem is solved to describe the relaxation of the resulted temperature field

$$\rho c_p \frac{\partial T}{\partial t} = \boldsymbol{\nabla} \cdot (\lambda \boldsymbol{\nabla} T), \quad \boldsymbol{x} \in \Omega^i, \tag{21}$$

$$-\lambda \boldsymbol{n} \cdot \boldsymbol{\nabla} T = \epsilon_T \sigma_{SB}(T^4 - T_{amb}^4) + k(T - T_{amb}), \quad \boldsymbol{x} \in \Gamma_1^i; \quad \lambda_l \boldsymbol{n} \cdot \boldsymbol{\nabla} T = 0, \quad \boldsymbol{x} \in \Gamma_2^i \cup \Gamma_{sym}^i, \tag{22}$$

$$T(t = 0) = T_{cld}^i, \quad \boldsymbol{x} \in \Omega^i, \tag{23}$$

after $\tau = 150$ s, during which the temperature field becomes almost uniform, where T_{cld}^i is temperature distribution in the structure immediately after surfacing the layer. The resulted temperature distribution is presented as an initial condition for solving the thermal conductivity problem when surfacing the next layer. Problems (15)–(20) and (21)–(23) are solved sequentially for each layer, taking into account changes in the initial conditions when adding a new layer.

The evolution of the temperature distribution during the successive surfacing of layers is shown in Fig. 5 at the moment of time immediately after the passage of the cross section by the heat source, and in Fig. 6, a at different times during the surfacing of the 10th layer. Fig. 6, b shows that, starting from the 5th layer, the temperature distribution along the z-axis practically becomes stationary in the coordinate system associated with the boundary of the deposited layer. At the same time, the maximum of this distribution turns out to be localised in 2–5 layers near this boundary due to the relatively low thermal conductivity of the materials. Fig. 6, c shows the dependence of temperature T_{rel}^i in the volume after relaxation on the number of the deposited layer, which has an extremum. Depending on the number of the deposited layer, the growth T_{rel}^i stops when the surface area that removes heat reaches a critical value.

4. Stress-strain state of the surfaced specimen after intermediate cooling

To describe the formation of residual stresses and eigenstrains in the wall on the substrate during exposure, a model of an isotropic thermo-elastic-plastic material was numerically implemented in the COMSOL Multiphysics software package. The standard model of large plastic and small elastic strains of metals was used in terms of the current Lagrangian approach in rates.
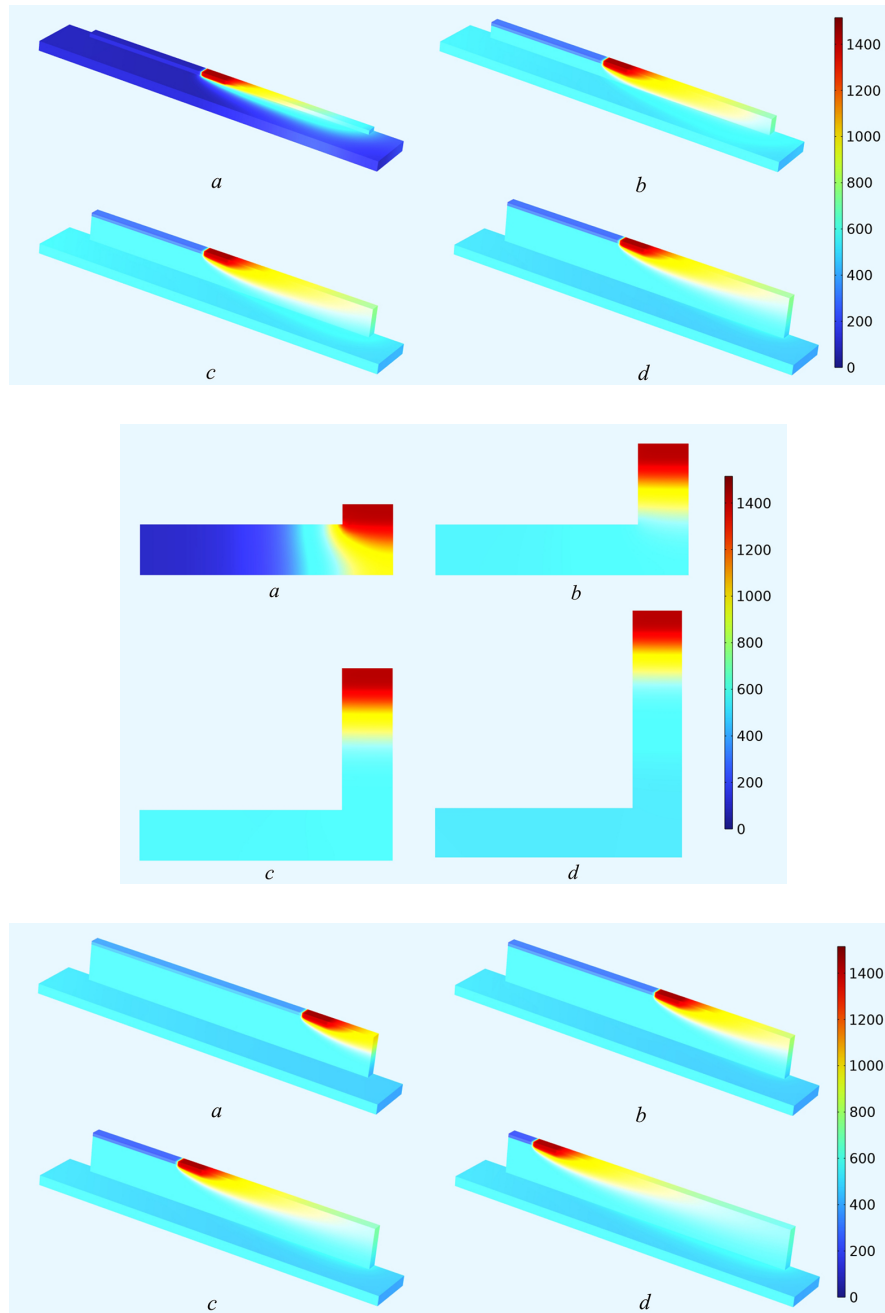
Fig. 5. Temperature distribution during the passage of the cross-section $x = 0$ (on top) and in the cross-section (in the middle) by the heat source during the surfacing of the layer: a) $i = 1$, b) $i = 4$, c) $i = 7$, d) $i = 10$ as far as during the surfacing of the 10th layer at time points: a) t = 4 s, b) t = 8 s, c) t = 12 s, d) t = 16 s (below)

The additivity of elastic, temperature and plastic velocity strain tensors is assumed, while the elastic one is associated linearly with the Jaumann derivative of the Kirchhoff stress tensor, and the plastic one $\dot{\epsilon}^p_{ij}$ with the Cauchy stress tensor σ_{ij}, i.e. the plastic flow rule associated with
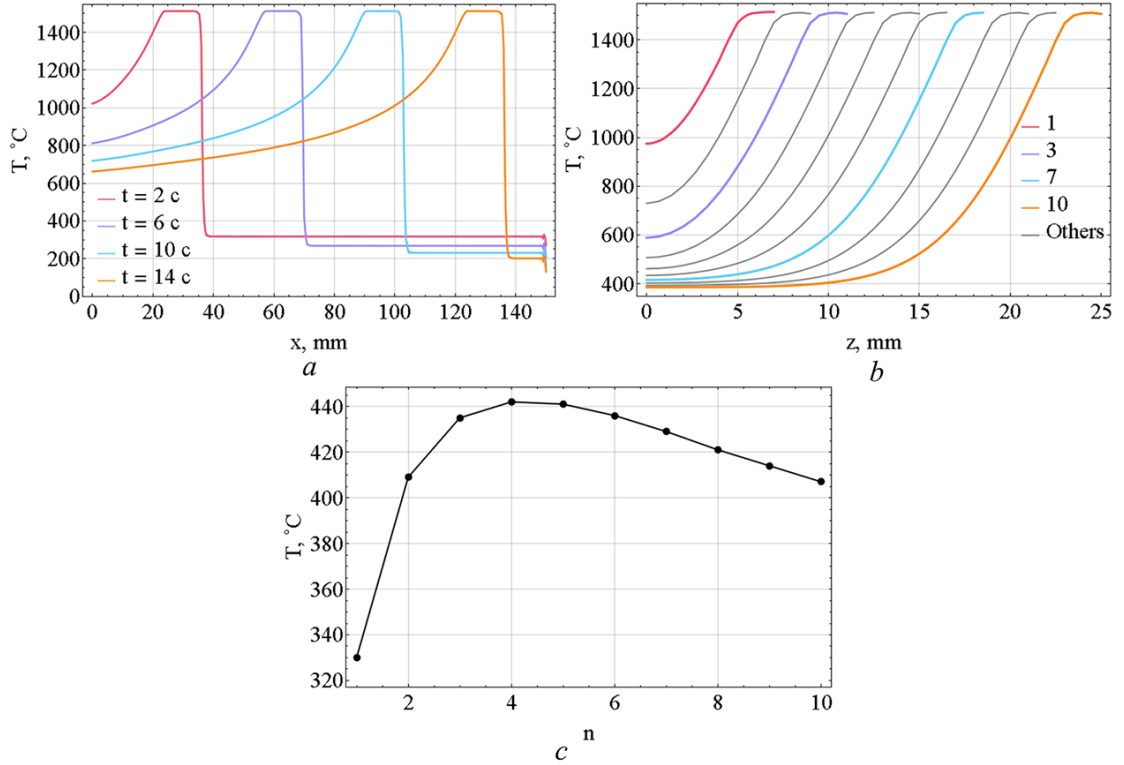
Fig. 6. Temperature profiles along the coordinate line z, $x = y = 0$ when surfacing each layer (a), y, $x = 0$, $z = z_9^{max}$ at various time points when surfacing the 10th layer (b) and Dependence of the temperature in the volume after relaxation T_{rel}^i on the number of the deposited layer (c)

the von Mises yield criterion

$$\dot{\epsilon}_{ij}^p = \dot{\lambda}\frac{\partial \phi}{\partial \sigma_{ij}}, \quad \phi = \frac{\sigma_M^2}{\sigma_u^2} - 1 = 0, \tag{24}$$

where $\sigma_M = \sqrt{3s_{ij}s_{ij}/2}$ is the Mises' stress intensity, $s_{ij} = \sigma_{ij} - \sigma_{kk}/3\delta_{ij}$ is the components of the stress deviator, σ_u is the yield stress under uniaxial tension, for which the Johnson–Cook isotropic hardening model is assumed as follows

$$\sigma_u = \left(A\left(1 + C\ln\frac{\dot{\epsilon}_p}{\dot{\epsilon}_*}\right) + B\left(1 + D\ln\frac{\dot{\epsilon}_p}{\dot{\epsilon}_*}\right)\epsilon_p^{n+\alpha\dot{\epsilon}_p} \right)k_u(T) \tag{25}$$

where $\epsilon_p = \int_0^t \dot{\epsilon}_p dt$ is the accumulated plastic strains, $\dot{\epsilon}_p = \sqrt{2\dot{\epsilon}_{ij}^p\dot{\epsilon}_{ij}^p/3}$ is the intensity of the plastic strain rates, $\dot{\epsilon}_* = 1\text{ s}^{-1}$ is the dimensional parameter.

The constants of the strain and speed hardening rule in (25) for the AISI 308 LSi steel were determined in [9]. The dependence of the temperature softening $E(T) = E_0 k_E(T)$ in (25) was taken in [10] for the EN 1.4301 steel, which was chemically close to AISI 308 LSi. It is assumed that the substrate steel behaves elastically, and the dependences of Young's modulus on temperature for both steels are also taken in [10]. The corresponding material constants and functions are given in Tab. 3. An implicit solver was used in the calculations.

Table 3. Constants of the thermoelastoplasticity model

Constant	Notion	Unit	Value
Constants of the hardening rule for AISI 308 LSi [9]	A	MPa	350
	C	–	0.106
	B	MPa	985
	D	–	0.56
	n	–	0.7
	γ	–	0.039
Young's modulus of AISI 308 LSi at 20°C	E_0	GPa	190
Young's modulus of the substrate steel at 20°C	E_0	GPa	210
Poisson's ratio of materials	ν	–	0.3
Density of materials	ρ	kg/m^3	7800
Coefficient of the linear thermal expansion of materials	α	K^{-1}	$18 \cdot 10^{-6}$

After relaxation for $\tau = 150$ s the temperature distribution $T(x,y,z) = T_{cld}^i(x,y,z)$ in the structure immediately after surfacing the layer becomes homogeneous $T(x,y,z) \equiv T_{rel}^i$ (Fig.6, a), and so induses inhomogeneous eigenstrains field $\epsilon_{ij}^{eig} = \alpha(T_{cld}^i(x,y,z) - T_{rel}^i)\delta_{ij}$. The thermo-elastic-plastic problem of forming the distribution of residual stresses and plastic strains in the structure caused by the thermal eigenstrains was solved. Fig. 7 shows the distributions of the x-components of eigenstrains and residual stresses tensor after surfacing of the ten-layer wall on a substrate and 150 s relaxation of the temperature field.
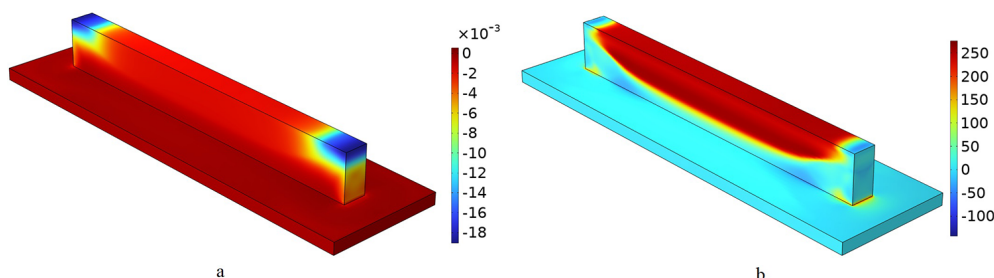

Fig. 7. The compressed eigenstrain (a) and tensile residual stress (b) x-components of deposited wall on a substrate after 150 s cooling

On the upper face of the wall, compressive total inelastic eigenstrains are quite inhomogeneously distributed along the length. Tensile stresses x-component the middle part of the specimen along its length at a depth of approximately five layers reach the yield stress of AISI 308 LSi steel at temperature T_{rel}^{10} and local magnitude of deformation hardening, providing a stress state close to the yield surface in the "stretching" direction of the stress space. Fig. 8 shows that plastic strains practically compensated for temperature eigenstrains in the middle cross-section of the specimen, leaving the value $\epsilon_x \approx 0.13\%$.

5.   Modelling of the specimen forging

To describe the wall forging the material model described in the previous section under dynamic approach was realized in the LS-DYNA package, where it corresponds to the standard material MAT_098 [11]. To regularise the problem in accordance with the recommendations given
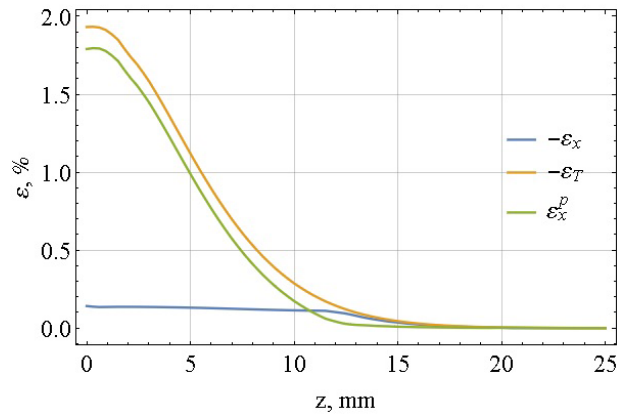
Fig. 8. Distribution of three components of inelastic eigenstrains along z-coordinate in the middle cross-section of the specimen

by the package developers, the Rayleigh damping coefficient $\beta = 0.1$ s was selected to provide the filtering of high-frequency harmonics and accelerate the calculation. The characteristic size of the finite elements (the hexagonal ones with the first order of approximation for volumes and the mesh ones for the contact surfaces of the head and stopper) was 1 mm.

The forging device in the numerical model consisted of an absolutely rigid head weighing $m = 0.5$ kg and connected to a fixed point by a spring of $k = 2.1$ N/m in rigidity and a damper with viscosity of $\mu = 3.1$ N·s/m. During the 1/100 period of the device (frequency $\nu = 47$ Hz), a force of $F_0 = 10$ kN was applied to the head. To calibrate the parameters of the device's effect on the workpiece, the strains of the control samples made of aluminum alloy AlMg5 and austenitic stainless steel 12Chr18Ni10Ti were matched to experimental values [12] (Fig. 9).
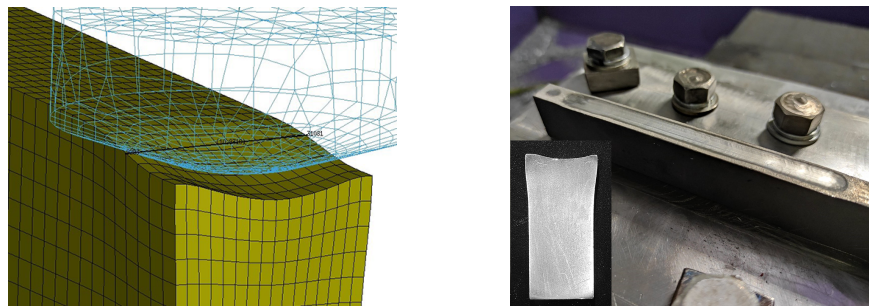

Fig. 9. Comparison of hammer impact in a numerical model by a control experiment

A single forging of a prestressed ten-layer wall after 150 seconds of relaxation of the temperature field leads to the development of the x-component of tensile plastic strain near the forging surface. As a result, the compressive eigenstrains localized near this surface partially disappear, reducing the source of the longitudinal bending of the structure when it is released. It should be noted that the transverse strains are at least an order of magnitude greater than the longitudinal ones, which is typical for point pressure treatment schemes of a linear segment. At the same time, forging the edge on the base without initial stresses can cause tensile or compressive longitudinal plastic strain near the forging surface [12, 13].

6.   Modelling the distortions of released specimen

A deflection of the specimen released from fastening at room temperature was calculated numerically in the COMSOL Multiphysics package in elasto-plastic approach given in Sect. 5. Fig. 10 shows the x-component stress field and the longitudinal bending of the specimen that occur when it is released after a) surfacing ten layers and cooling to room temperature and b) surfacing ten layers, relaxation, single forging and cooling to room temperature. In the first case, the amount of deflection was $D = 1.85$ mm, and in the second one $D = 0.35$ mm. It is possible to note some intricate change in the distribution of residual stresses along the wall height.
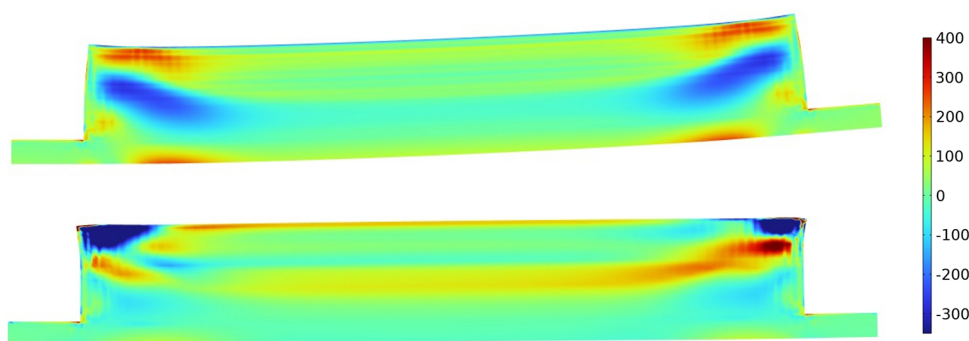

Fig. 10.   X-component stress field in the plane of symmetry after releasing of the deposited specimen a) without forging, b) with single forging

Fig. 11 shows the results of calculating the deflection of the released specimen depending on the number of deposited layers according to the beam-rod model. The data from Tab. 4

Table 4. Constants of the beam-rod model

Constant	Notation	Unit	Value
Thermal expansion coefficient	α	K^{-1}	$18 \cdot 10^{-1}$
Elasticity modula	$E_s = E_l$	GPa	200
Substrate width	B	mm	50
Substrate thickness	H	mm	5
Substrate length	L	mm	180
Layer width	b	mm	10
Layer thickness	h	mm	2
Layer length	l	mm	150
Temperature of the upper and the next layer	$T_1,\ T_2$	K	1788
Temperature in the remaining layers	$T_i,\ i = 3, \dots, n+1$	K	673
Ambient temperature	T_{amb}	K	293

was used. Due to the heterogeneity of the distribution of eigenstrains along the length of the wall, in order to match the deflection of the specimen according to the beam-rod model to the experimental (1.95 mm) or calculated (1.85 mm) values, the amounts of ϵ_i^t, $i = 1, \dots, n+1$ had to be adjusted. To match the deflection value $D = 1.85$ mm, the rough profile $\epsilon_i^t = -0.73\%$, $i = 1, \dots, 5$, $\epsilon_i^t = 0$, $i = 6, \dots, 11$ was set. The dependences in Fig. 11 allow us to understand

how the deflection and the average longitudinal strain of the specimen changes depending on the number of deposited layers, as well as the distribution of eigenstrains along the thickness of the ten-layer wall on the substrate. The nonmonotonicity of the dependence of the deflection of the specimen on the number of deposited layers is noteworthy, reaching a maximum of $D = 3.89$ mm at $n = 3$. The break/discontinuity in the curves of ϵ_n and ϵ^{eig} are associated with the ramp-shape of the profile ϵ_i^t, which is easier to adjust. It should be noted that this feature does not manifest itself in any way on the dependence of the deflection of the specimen. In Fig. 11 the results of numerical calculation of all values in the COMSOL Multiphysics package in elastic formulation are also given, which allow us to evaluate the accuracy of the beam-rod model in relation to the structure under consideration.
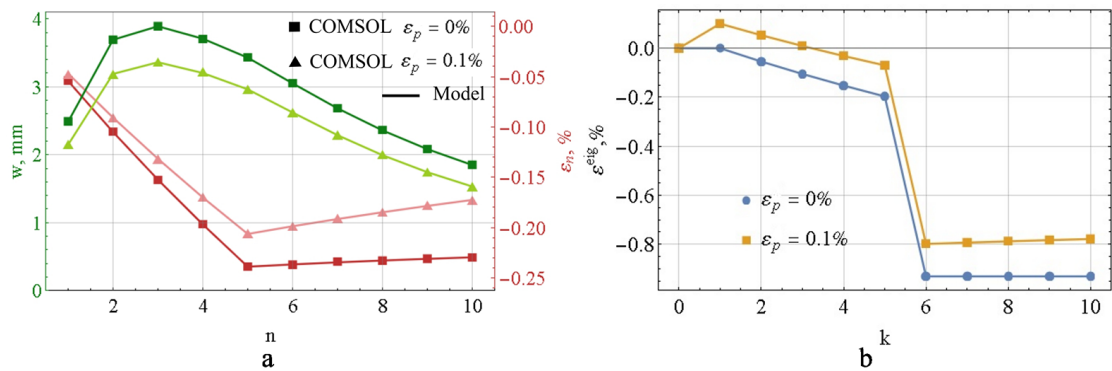

Fig. 11. Dependence of the longitudinal strains and the deflection of the specimen on the number of layers to be deposited (a) and eigenstrains in ten-layers specimen (b) at two values of plastic strains during layer-by-layer forging

Fig. 11 also shows the data for calculating the deflection of a sample grown with layer-by-layer forging. To do this, a value $\epsilon^p = 0.10\%$ was set for which the deflection of the specimen coincided with the experimental one $D = 1.53$ mm. Forging does not significantly affect the qualitative form of the dependence of the deflection of the specimen on the number of deposited layers; the maximum deflection $D = 3.36$ mm at $n = 3$ is slightly reduced in this case.

Conclusions

This article considers the specimen consisting of a wall deposited on a fixed substrate [7] to analyse the distortions of a metal structure built by additive manufacturing and the distribution of residual stresses in it. Wire-arc surfacing wall of stainless steel AISI 308 LSi with and without layer-by-layer forging, for which the deflection of was measured. A numerical model of the process was constructed and verified, including the stages of workpiece surfacing and intermediate cooling (thermal problem), changes in stresses and strains during the cooling, its forging using a pneumatic tool and its release from fastenings (thermo-elastic-plastic problems). The calculated deflections of the specimen surfaced without intermediate forging are consistent with the experiment. As an alternative to the numerical solution of the latter problem, we proposed and verified a beam-rod elastic model for estimating the deflection of the specimen and the distribution of residual stresses and eigenstrains along the wall height. It is established that the occurrence of plastic strains during the cooling of the specimen leads to heterogeneity of the dis-

tribution of eigenstrains along it and does not allow comparing the beam-rod model to numerical elastic-plastic calculation. Nevertheless, the beam-rod model can be used to describe the laws of variation of these quantities, taking into account the peculiarities of the mechanics of the body being built up. This is required to select rational parameters of the technological process, in particular, the relaxation time after surfacing and the intensity of layer-by-layer pressure treatment, to minimise the structure distortion and the nonuniform distribution of residual stresses.

References

[1] J.Gu, X.Wang, J.Bai, J.Ding, S.W.Williams, Y.Zhai, K.Liu, Deformation Microstructures and Strengthening Mechanisms for the Wire – Arc Additively Manufactured Al-Mg4.5Mn Alloy with Inter-Layer Rolling, *Mater. Sci. Eng.*, **A712**(2018), 292–301.
DOI: 10.1016/j.msea.2017.11.113

[2] J.R.Honnige, P.A.Colegrove, S.Ganguly, E.Eimer, S.Kabra, S.W.Williams, Control of Residual Stress and Distortion in Aluminium Wire – Arc Additive Manufacture with Rolling, *Additive Manufacturing*, **22**(2018), 775–783. DOI: 10.1016/j.addma.2018.06.015

[3] K.P.Karunakaran, S.Kapil, S Negi, Multi-Station Multi-Axis Hybrid Layered Manufacturing System, Indian Patent no. 201821038516, 2018.

[4] Y.Shchitsyn, M.Kartashev, E.Krivonosova, T.Olshanskaya, D.Trushnikov, Formation of Structure and Properties of Two-Phase Ti-6Al-4V Alloy during Cold Metal Transfer Additive Deposition with Interpass Forging, *Materials*, **14**(2021), no. 16, art. 4415.
DOI: 10.3390/ma14164415

[5] D.N.Trushnikov, M.F.Kartashev, T.V.Olshanskaya, M.R.Mindibaev, Y.D.Shchitsyn, F.R.Saucedo-Zendejo, Improving VT6 Titanium-Alloy Components Produced by Multilayer Surfacing, *Russian Engineering Research*, **41**(2021), no. 9, 848–850.
DOI: 10.3103/S1068798X21090264

[6] A.Kirichek, O.Fedonin, A.Khandozhko, A.Zhirkov, D.Soloviyov, S.Barinov, Hybrid Technologies and Technical Equipment for Additive Synthesis of Products, *Science Intensive Technologies in Mechanical Engineering*, (2022), no. 8, 31–38.
DOI: 10.30987/2223-4608-2022-8-31-38

[7] J.Hoennige, C.Er Seow, S.Ganguly, X.Xu, S.Cabeza, H.Coules, S.Williams, Study of Residual Stress and Microstructural Evolution in As-Deposited and Inter-Pass Rolled Wire Plus Arc Additively Manufactured Inconel 718 Alloy after Ageing Treatment, *Mater. Sci. Eng.*, **A801**(2021), art. 140368. DOI: 10.1016/j.msea.2020.140368

[8] A.V.Manzhirov, General Inertia-Free Initial Boundary Value Problem for a Piecewise Continuously Increasing Viscoelastic Aging Body, *J. Appl. Math. Mech.*, **59**(1995), no. 5, 836–848 (in Russian).

[9] Yu.V.Bayandin and ets., Strength and Ductility Characteristics of Metal Alloys and Stainless Steels Created by Wire-Arc Surfacing in a Wide Range of Strain Rates, *PNRPU Mechanics Bulletin*, (2023), no. 1, 33–45 (in Russian). DOI: 10.15593/perm.mech/2023.1.04

[10] EN 1993-1-2:2005 Eurocode 3: Design of steel structures. Part 1-2: General rules – Structural fire Design, CEN, 2005.

[11] LS-DYNA$^{®}$ Keyword User's Manual. Volume II. Material Models. Ver. R13, LSTC, 2021.

[12] I.E.Keller, A.V.Kazantsev, D.S.Dudin, G.L.Permyakov, M.F.Kartashev, Shape distortions, plastic strains and residual stresses after one-sided forging/rolling of the beam: application to additive manufacturing of the linear metal segment with layer-by-layer pressure treatment, *Computational Continuum Mechanics*, **14**(2021), no. 4, 434–443.
DOI: 10.1016/j.msea.2020.140368

[13] I.E.Keller, D.S.Petukhov, D.S.Dudin, G.L.Permyakov, D.N.Trushnikov, Method for Determining Residual Stresses in a Rib on a Rigid Base, Russian Patent no. 27977712018, 2023.

Моделирование остаточных напряжений и искажений стенки на подложке, возведенной проволочно-дуговой наплавкой

Дмитрий С. Дудин
Илья Э. Келлер
Институт механики сплошных сред УрО РАН
Пермский национальный исследовательский политехнический университет
Пермь, Российская Федерация
Глеб Л. Пермяков
Дмитрий Н. Трушников
Пермский национальный исследовательский политехнический университет
Пермь, Российская Федерация

Аннотация. Для исследования формирования остаточных напряжений и искажений изделий, создаваемых проволочно-дуговой наплавкой, в зависимости от параметров технологического процесса предложено рассматривать стенку, состоящую из десяти слоев, наплавленных на подложку. На закрепленной стальной пластине проволокой из аустенитной нержавеющей стали AISI 308 LSi наплавлена стенка с послойной проковкой и без нее и измерен прогиб освобожденной конструкции. Для численного моделирования процесс представлялся в виде последовательно решаемых задач: а) тепловой — наплавки десяти слоев материала, б) упругопластической — формирования собственных деформаций и остаточных напряжений вследствие остывания созданной конструкции с неоднородным распределением температуры, в) упругопластической — проковки напряженной заготовки пневмоинструментом при повышенной температуре (этап может отсутствовать) и г) упругопластической — искажения конструкции и изменения поля остаточных напряжений при освобождении конструкции. Задачи (а), (б) и (г) решались в пакете программ COMSOL Multiphysics, (в) — в LS-DYNA. Установлено, что в наплавленной стенке вблизи ее верхней грани формируются растягивающие остаточные напряжения, а проковка этой грани сопровождается уменьшением продольных деформаций, искажения освобожденного образца и неоднородности распределения остаточных напряжений по высоте стенки. Рассчитанные величины прогибов соответствуют нашим экспериментальным данным и результатам Университета Крэнфилда для аустенитного сплава IN718. Разработана балочно-стержневая модель механики наращиваемой многослойной стенки, результаты применения которой соответствуют численным расчетам.

Ключевые слова: проволочно-дуговая наплавка, послойная проковка, остаточные напряжения, искажения, эксперимент, математическая модель.